Food Control 182 (2026) 111861

Contents lists available at ScienceDirect

Food Control

journal homepage: www.elsevier.com/locate/foodcont

Meat superchilling monitoring by NIR: penetration limits and multivariate charts

Irene Locatelli, Silvia Grassi *

Department of Food, Environmental and Nutritional Sciences, University of Milan, Via Celoria 2, 20133, Milano, Italy

ARTICLE INFO

Keywords:
Near-infrared spectroscopy
NIR penetration depth
Superchilling monitoring
Multivariate statistical control charts

ABSTRACT

Near-infrared spectroscopy offers promising non-destructive monitoring for food processing, but its effectiveness depends on both signal penetration and real-time detection of physiochemical changes. Therefore, this study investigates three key aspects of NIR application in meat superchilling: (i) assessing the thermal stability of the MicroNIR device under process conditions, (ii) evaluating the penetration depth of NIR signal in pork, beef and chicken tissues, and (iii) developing multivariate statistical control charts (MSCC) to monitor freezing dynamics through water-related spectral changes.

Penetration depth was assessed by placing meat slices (2.5–30 mm) between polypropylene and a MicroNIR sensor, determining the maximum detectable depth. In a parallel experiment, cubed meat samples (30 × 30 × 30 mm) underwent controlled superchilling with spectra collected every 2 min and analysed through principal component analysis (PCA) and aquaphotomics.

The MicroNIR demonstrated signal stability under varying temperature conditions, confirming its suitability for in-line monitoring. Results showed NIR penetrates up to 5 mm under refrigeration conditions, with reduced effectiveness under freezing. However, this was enough to detect the thin frozen surface layer characteristic of superchilling. Spectral variations during the process showed consistent trends, particularly in the water-related band. PCA highlighted key water phase transitions, while aquagrams mapped water structuring. MSCCs based on PCA and aquaphotomic markers reliably identified superchilling start and end in real time, closely matching temperature-based references.

This work not only clarifies the effective penetration limits of NIR in refrigerated and frozen muscle tissues, but also proposes a robust, automatable strategy for process monitoring based on the spectral behaviour of water.

1. Introduction

In recent years, the global food industry has faced challenges related to inefficient refrigeration management along the cold chain, leading to alarming levels of food waste. Estimates suggest that a considerable proportion of food production is lost during storage and transport due to inadequate temperature control, highlighting the critical need for improved preservation strategies (Shiraishi et al., 2025).

In response to this issue, superchilling has emerged as a promising technique for preserving meat product, offering a potential solution to reduce food waste. This technique maintains food at temperatures just below its freezing point, effectively extending shelf life during storage, transport and retail (Banerjee and Maheswarappa, 2019). Superchilling not only maintains food freshness and preserves high quality but also suppresses the growth of harmful microbes. Furthermore, it reduces the need for traditional freezing and thawing processes, thereby increasing yield and reducing energy, labour, and transport costs (Kaale et al., 2011). Compared to other preservation methods such as conventional refrigeration and freezing, superchilling offers a balanced approach that prevents the degradation of texture and quality often observed in frozen products (Kaale et al., 2011).

Existing research has investigated the advantages of superchilling, particularly regarding the preservation of the quality and freshness of meat and fish products. For instance, Ding et al. (2020) examined the effects of various levels of superchilling on pork, demonstrating that a high degree of superchilling can extend the shelf life of pork while maintaining superior meat quality. However, findings by Kim and Hong, 2022 suggest that while superchilling may not be ideal for preserving beef quality, it can effectively extend the freshness of beef sirloin. De Rezende et al. (2022) highlights that various parameter considered

* Corresponding author.
E-mail address: silvia.grassi@unimi.it (S. Grassi).

https://doi.org/10.1016/j.foodcont.2025.111861
Received 15 September 2025; Received in revised form 11 November 2025; Accepted 17 November 2025
Available online 21 November 2025

during superchilling, applied to seafood products (e.g., technique intensity, applied temperatures, amount of water cooled below the freezing point) influence quality outcomes. Nevertheless, superchilling results in a significantly longer shelf life compared to regular refrigeration.

Despite relevant progress in understanding superchilling mechanisms and their effects on product quality, most existing studies have focused on evaluating quality under controlled or static storage conditions. However, few researches have addressed the dynamic aspects of the chilling processing phase through real-time monitoring approaches (Magnussen et al., 2008). In particular, current analytical methods often remain inadequate for providing continuous monitoring throughout the superchilling process, hindering the ability to maintain consistent and optimal conditions during processing (Banerjee and Maheswarappa, 2019). Moreover, maintaining stable thermal conditions is crucial during superchilling, as even slight temperature fluctuations or inconsistent cooling rates may lead to extensive ice recrystallization phenomena, negatively impacting the texture and overall quality of the meat (Wang et al., 2024). This gap creates significant obstacles in realizing the full potential of superchilling for extending shelf life and reducing food waste in industrial-scale operations.

To address this challenge, the introduction of online measurement techniques, such as Near-Infrared Spectroscopy (NIR), is essential to monitor and control the ice fraction in specific products during superchilling, thus optimizing the process and ensuring consistent product quality (Grassi et al., 2024; Stevik et al., 2010).

The basis of the study relies on the fact that NIR spectra are affected by temperature dependence of water molecule absorption in the near-infrared region. As first systematically analysed by Collins (1925), temperature variations induce both shifts in the position, and changes in the intensity and shape of water absorption bands. This is due to the modifications in hydrogen bonding and in molecular vibrational states (Maeda et al., 1995). These are also the basis of aquaphotomics (Tsenkova et al., 2018). In the context of superchilling processes, these changes are critical, as they reflect temperature-induced alterations in the physical state of water within the sample surface.

Nevertheless, two important factors must be considered when implementing NIR as a PAT tool for superchilling monitoring: the influence of temperature on the instrument subjected to temperature changes and the penetration dept of the radiation.

Indeed, NIR instruments, particularly the miniaturized portable instruments, lack of thermal management, thus being sensitive to ambient temperature fluctuations (Ramadan et al., 2025). To minimize instrumental artefacts, mathematical correction could be implemented directly by the software, thus the retrieved measured absorbance is already corrected; or via subsequent spectra correction during model development, such as orthogonal projection (Roger & Boulet, 2018). In any case, this effect must be ruled out to ensure the reliability of the developed monitoring models.

Furthermore, the effectiveness of NIR spectroscopy depends on the ability of the radiation to penetrate biological tissues, affecting the depth of analysis and therefore the representativeness of the signal collected. Penetration varies depending on wavelength, tissue absorption and scattering coefficients, and the optical configuration used (Huang et al., 2024; Lammertyn et al., 2000). While the literature has focused largely on light penetration in plant tissues such as fruit and vegetables, which are characterised by chemical and physical differences between the skin and pulp (Huang et al., 2024; Lammertyn et al., 2000), there is limited knowledge about NIR interaction with animal tissues. Research such as that conducted by Padalkar and Pleshko (2015) on cartilage highlights the gap that exists in the characterisation of the optical properties of animal tissues.

Understanding the penetration of NIR radiation in muscle tissues is crucial because it directly affects the representativeness and reliability of the spectroscopic signal. The penetration depth determines which tissue layers contribute to the signal, influencing the accuracy of detecting physical and chemical changes such as water state transitions during superchilling conservation (Deepika & Sutar, 2024; Huang et al., 2024). A lack of penetration depth knowledge may lead to misleading interpretations or insufficient sensitivity in monitoring applications. Therefore, characterizing NIR penetration in muscle tissues enables better calibration, selection of optimal wavelengths, and development of robust real-time monitoring systems for meat preservation. The present study aims to fill these gaps by studying: (i) the effect of temperature fluctuation on MicroNIR sensor and not related to water changes, (ii) the depth of penetration of MicroNIR radiation in beef, pork and poultry tissues. After setting these bases, the research focused on the development of a dynamic monitoring system based on multivariate analysis (PCA) and aquaphotomics for real-time detection of water transitions during superchilling. Through this approach, the operational limits of NIR spectroscopy applied to muscle tissues are defined, and a robust and automatable strategy for continuous control of the preservation process is proposed.

2. Materials and methods

2.1. Experimental set up

Three cuts of fresh meat - pork loin, chicken breast, and beef rump - were purchased from Italian local markets and analysed one day after the industrial sectioning during which the cuts were stored at 4 ± 1 °C. Pork loin was purchased in two batches (4517168, 4517427) prepared on the February 11, 2025 and the March 09, 2025 by C.E.M. COOP. ESERCENTI MACELLAI – SOCIETÀ COOPERATIVA (Cesena, Italy) with UE IT 1477S authorisation. Chicken breast was purchased in two batches (405840, 406333) prepared on the November 07, 2024 and on the December 15, 2024 by Carni SOC COOP Agr. (Ancona, Italy) with UE IT 0194M authorisation. Beef rump was purchased in two batches (00000947, 00000558) prepared on the November 10, 2024 and the January 15, 2025 by FIORANI E C. SPA (Piacenza, Italy) with UE IT592S authorisation.

The experimental work was divided into three main investigations:

- NIR signal stability in the process analytical technology (PAT) set up:

A green polypropylene (PP) material was placed on the top of the MicroNIR device placed inside the air flow maintained at −18 °C and a speed of 1.3 m/s. Spectral measurements were collected under controlled thermal conditions, over a monitoring period of approximately 2 h.

- NIR signal penetration assessment:

For each meat cut, different slices were prepared with fixed surface dimensions of 30 × 30 mm and variable thicknesses of 30, 20, 10, 5, and 2.5 mm. These samples were placed between the MicroNIR sensor and a green PP material to evaluate the effective penetration depth of the NIR signal.

Spectral measurements were collected under controlled thermal conditions, ranging from refrigerated to frozen states, over a monitoring period of approximately 2 h.

- Superchilling process monitoring (Fig. 1):

To account for biological and anatomical variability, two separate cuts were selected for each meat type. From each cut, two to three cubes measuring 30 × 30 × 30 mm were obtained, resulting in five samples per meat cut. All samples were wrapped in transparent PVC film to simulate packaging conditions and to prevent direct contact with the NIR sensor during acquisition. These cubes were then monitored throughout the ice crystallisation, up to 120 min.

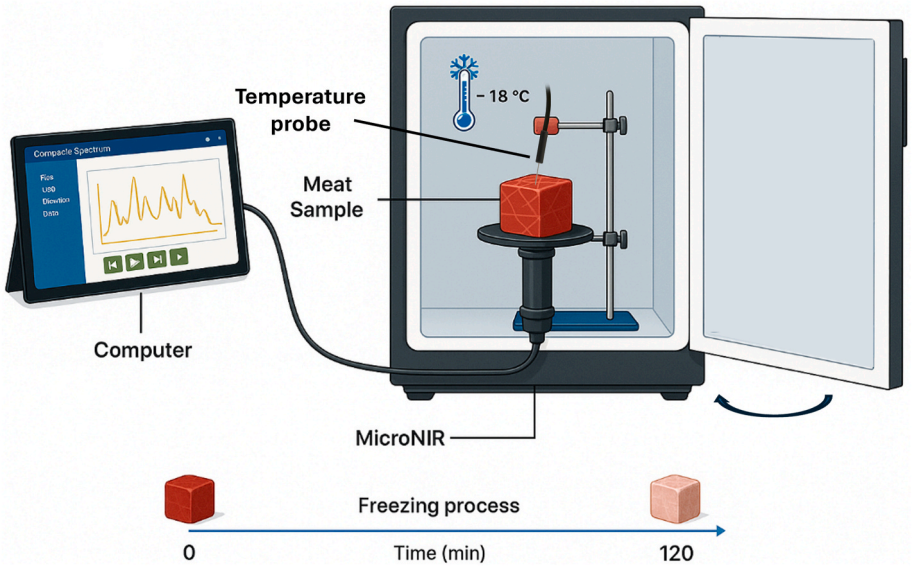

Fig. 1. Schematic representation of the experimental setup for superchilling monitoring.

2.1.1. NIR signal stability in the PAT set up

To evaluate the reliability of the MicroNIR (Viavi Solutions, USA) signal at sensor temperature variation, a green PP material was analysed following two procedures. Indeed MicroNIR, equipped with an uncooled InGaAs detector, could be sensitive to temperature changes. Even though, these instruments are programmed with a set of temperature correction factors that mitigates this effect.

Firstly, the MicroNIR was calibrated by dark and reference (Spectralon™) after the sensor temperature reached 16 °C inside the freezing chamber. After the calibration, the spectral measurements of the PP material placed on the sensor were recorded with an integration time of 12.5 ms and automatic scans every 120 s. The acquired spectra covered a range of 950–1650 nm with a resolution of 6.2 nm every. With this setup the dark background and reference are restored by default functionality to permit acquisition of sample spectra when the MicroNIR is mounted in a process.

Moreover, the effect of MicroNIR sensor temperature on the dark and reference was investigated. The PP material spectra were acquired along the same PAT setup; however the dark and reference were recorded at different temperatures (from 16 °C to −7 °C with interval of 3 °C) by stopping the data collection in-between.

2.1.2. Evaluation of NIR signal penetration depth

The penetration depth of NIR was evaluated by placing each sample between the MicroNIR sensor (Viavi Solutions, USA), operating in the 950–1650 nm spectral range (12.5 ms integration time and 120 number of scans), and a green polypropylene sheet placed on the opposite side. This configuration was used to verify whether NIR radiation was able to completely penetrate the muscle tissue and detect the spectral signature of the PP sheet positioned below.

Spectral measurements were collected every 120 s during a controlled cooling process (air flow maintained at −18 °C and a speed of 1.3 m/s), as the samples transitioned from refrigeration to freezing conditions. A reference spectrum was collected from the PP plate to identify any peaks of interest.

The raw spectra were pre-processed by applying smoothing (Savitzky Golay, 3 window points, third polynomial order) and Standard Normal Variate (SNV) transformation or first derivative (d1, Savitzky Golay, 3 window points, third polynomial order) calculation to improve spectral resolution and reduce baseline shifts. Prior to PCA each dataset was mean centred.

PCA, a widely recognised unsupervised exploratory method (Wold et al., 1987), was then performed using MATLAB (v. 2017b) and PLS Toolbox (v. 8.5, Eigenvector Research, Inc.) to study the spectral differences associated with sample thickness and temperature and to determine the detectability of the PP material signal.

2.2. Superchilling process monitoring and data analysis

The same superchilling setup and spectra acquisition mode were performed for process monitoring, adding a temperature sensor (Elitech GSP-6, UK) in the geometrical centre of the meat sample. Moreover, the samples were wrapped in transparent PVC film.

The preprocesed spectra were explored by PCA as described above with the purpose of studying spectral changes during superchilling and to evaluate sample variability. Furthermore, aquagrams were calculated following the classical procedure described by Tsenkova et al. (2018) to visually depict spectral patterns related to water. These tools are valuable for understanding the structural changes of water within a system, with axes representing different molecular conformations. Key absorbance bands of water were selected, following protocols from Tsenkova et al. (2018) and Kovacs et al. (2022), to ensure relevance and reproducibility. The number of aquagram axes was tailored to the specific experimental system and perturbation, emphasizing the most informative spectral features.

The aquagram visualisation was designed to monitor temporal changes in water state during the superchilling process, offering a dynamic perspective on water structure and its transformations. This approach enabled a comprehensive analysis of water behaviour along the process progress.

3. Results and discussion

3.1. MicroNIR signal stability at PAT conditions

The stability of the MicroNIR signal under PAT conditions was evaluated by PCA on a combined dataset including (i) five samples per matrix (pork loin, chicken breast, beef rump) used in the process study and (ii) stability tests performed on PP reference material in continuous and discontinuous acquisition modes. All spectra were pretreated with smoothing, SNV, and mean centering before analysis.

In the score plots (Fig. 2A and C), PC1 described the main source of variability associated with the phase transition of water from free (liquid) to bound (ice), with an evolution from positive to negative

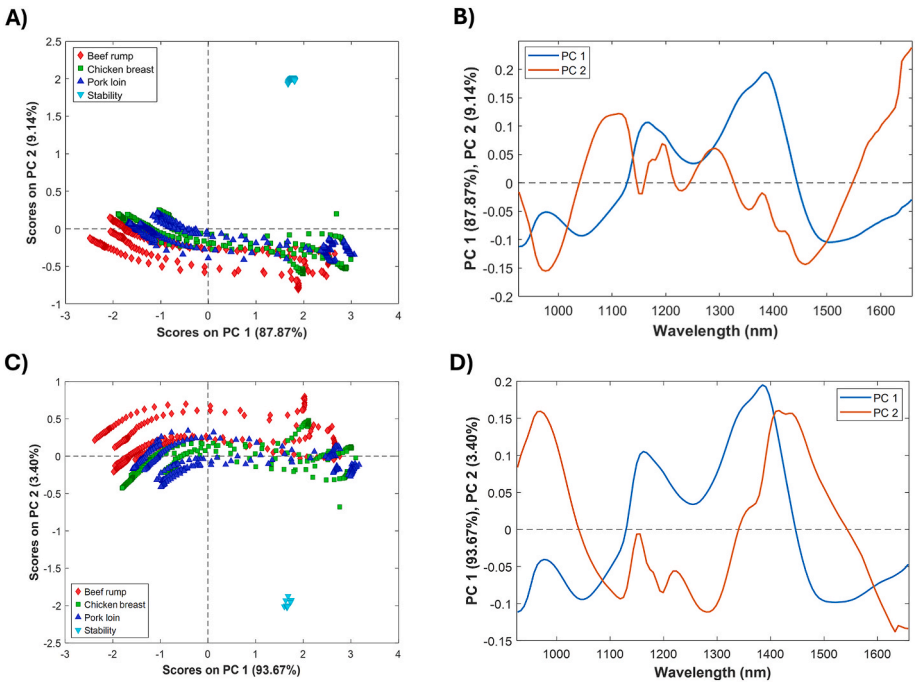

Fig. 2. Score plot (A, C) and loading plot (B, D) plots of the combined dataset of meat samples and the polypropylene (PP) reference, obtained under continuous (A, B) and discontinuous (C, D) acquisition modes, during the MicroNIR signal stability study. Spectra pretreated with smoothing (3 pt) and SNV.

values as freezing progressed in the meat samples. The trend observed in the score plots is consistent with the contributions of PC1 loadings (Fig. 2B and D), which show pronounced bands around ~980 nm, ~1168–1170 nm, and ~1400–1460 nm, typical of the OH vibrations of water. This behavior, common to all the analysed matrices, will be further explored in Section 3.3 in relation to the superchilling dynamics.

PC2 mainly described the spectral contribution of the reference material (PP). In particular, the spectra acquired during the continuous test are located at strongly positive PC2 (9 % of the total variance) values, while those obtained in the discontinuous mode are located at strongly negative PC2 (3 % of the total variance) values, clearly separating from the meat samples. The PC2 loadings are characterized by a signal at ~1416 nm consistent with the absorption band of PP (Masoumi et al., 2012).

It is important to note that no drift along PC1 was observed in the PP tests, unlike in the meat samples where the progressive shift in scores reflects changes in water molecular vibrational states. This behavior confirms that the MicroNIR maintains signal stability even when the sensor temperature varies, and that the spectral variations associated with freezing are attributable exclusively to the sample properties. Therefore, the instrumental setup can be considered reliable and suitable for in-line monitoring of the superchilling process.

3.2. MicroNIR signal penetration depth

The ability of the NIR signal to penetrate muscle tissue was assessed by analysing the spectral responses on samples of pork loin, chicken breast and beef rump of different thicknesses (30, 20, 10, 5 and 2.5 mm), both in refrigerated and frozen conditions.

Fig. 3 shows NIR spectra, pre-treated with SNV and d1, of pork loin slices of five different thicknesses positioned between the MicroNIR sensor and the PP sheet, acquired under two thermal conditions: refrigerated (~4 °C, Fig. 3A) and frozen (internal temperature below −4 °C, Fig. 3B). The spectrum of the PP sheet alone is also displayed (black line).

As reported by Masoumi et al. (2012), PP exhibits characteristic absorption peaks at 1199 nm and 1394 nm in untreated NIR spectra. While derivative preprocessing alters the spectral shape, these wavelengths continue to be useful as reference points to interpret features in transformed spectra.

Under refrigeration conditions (Fig. 3A), the contribution of the PP signal is detectable through the thinnest sample (2.5 mm), as indicated

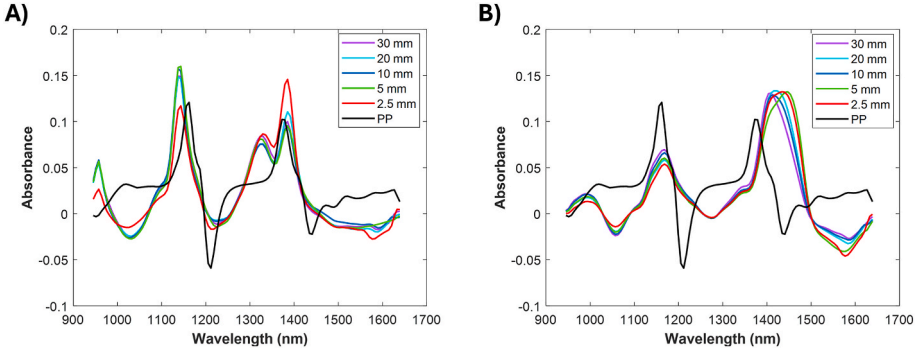

Fig. 3. NIR Spectra collected during the MicroNIR signa penetration depth study at one point of refrigerated (A) and frozen (B) process of pork loin, pretreated with smoothing (3 pt), and 1st derivative.

by the spectral similarity around 1211 nm. As thickness increases, this signal progressively attenuates. Beyond 5.0 mm, PP-related features are no longer visible, suggesting that the NIR radiation is either absorbed or scattered before reaching the underlying PP sheet. These results indicate a penetration depth between 2.5 and 5.0 mm, in line with previous observations in other biological tissues (Padalkar & Pleshko, 2015).

In frozen samples (Fig. 3B), the spectral profiles differ due to water phase transitions and the alteration in tissue structure. The formation of ice crystals leads to increase scattering and reduce transparency, further attenuating the NIR signal transmission. Even in the thinnest sample (2.5 mm), the PP signal is nearly detectable, confirming that the thermal state of the sample affects penetration ability.

This behaviour was further explored through PCA on SNV-transformed spectra (Fig. 4), aiming to study the combined influence of tissue thickness and thermal state on NIR signal transmission. The score plot of PC1 vs PC2 (Fig. 4A) revealed two main gradients: the main one (94.35 % of explained variance) corresponding to changes in water physical state on the product surface, and a secondary one (3.1 % of total variance) one associate with sample thickness. Spectra acquired during the early refrigeration stages are located on the right side of the PC1 axis (positive value), while those acquired later shift progressively leftward, indicating a transition to a frozen state.

PC1 explained most of the total variance and appeared to reflect changes related to the thermal-induced change in the tissue. The gradual shift of all samples along PC1 reflects the phase transition of water, as ice formation alters the NIR spectral response. The corresponding loadings plot (Fig. 4B) shows peaks at approximately 980, 1168, and 1400 nm, which are associated with key water-related absorbances: 980 nm corresponds to the second overtone of OH stretching, while 1168 and 1400 nm relate to combination bands and the first overtone of OH stretching, respectively (Workman and Weyer, 2007). These spectral features confirm that PC1 captures the freezing dynamics, consistent with previous studies on frozen muscle tissue (Grassi et al., 2024; Workman & Weyer, 2007).

PC2, on the other hand, captured variability related to sample thickness and NIR penetration depth. At the beginning of the process, only the thinnest sample (2.5 mm) displayed positive PC2 values, whereas the thicker samples clustered at negative values. This separation likely reflects the presence or absence of spectral contribution from the underlying PP layer, detectable only through the thinnest slices. As the freezing process advanced, all samples converged towards similar PC2 values, suggesting that the formation of ice on the slice surface uniformly reduced NIR transmission, regardless of tissue thickness. The loadings for PC2, reinforce this interpretation: peaks at 1416 nm and a small inflection near 1200 nm, are consistent with the PP absorption bands described in literature (Masoumi et al., 2012). Their presence in PC2 indicates that this component captures penetration-related differences, confirming that PP detection was only possible in unfrozen-thin samples. Although pork loin was selected for illustration, similar behaviours were observed in chicken breast and beef rump, supporting the general validity of the observed penetration limit (Fig. S1). Despite the attenuation, this level of penetration remains suitable for monitoring the thin frozen layer (1–3 mm) that typically forms during superchilling (Kaale et al., 2013).

3.3. Superchilling process monitoring

3.3.1. Temperature profile

The temperature curves recorded during the five freezing tests for all three meat types (pork loin, chicken breast, and beef rump) displayed a typical freezing trend, characterised by the presence of a district 'thermal plateau' (Fig. 5). This plateau generally appeared in the temperature range between −0.5 °C and −1.5 °C and represents the phase change interval during which latent heat removal dominates the thermal exchange dynamics. This phenomenon reflects the heat associated with the phase transition of water to ice within the meat, rather than the sensible heat exchange between the product and the surrounding freezer air. The duration and extent of the plateau varied slightly depending on meat cut, due to compositional differences, but the underlying thermophysical behaviour was consistently observed across all tests.

3.3.2. NIR results

The NIR spectra collected throughout the process revealed consistent spectral patterns across all three meat cuts (Fig. 6). Each subplot (A, B, C) represents a single test for pork loin, chicken breast, and beef rump, respectively, and shows the changes in the spectral profile as freezing progresses.

In each case, the pre-treated spectra (SNV) showed prominent absorptions features around 980, 1170, and 1430 nm. These wavelengths are known to correspond to specific vibrational combinations of water molecule. In particular, the peak near 980 nm is associated with the second overtone of the OH stretching band (3ν1.3), the absorption at 1170 nm and 1430 nm are attributed to a combination of the first overtone of the OH stretching band and the OH bending band (2ν1.3 + ν2), and the first overtone of the OH stretching band (2ν1.3) (Workman and Weyer, 2007). A systematic shift in these peaks was observed as the temperature of the sample decreased during freezing; specifically, the water-related absorption bands shifted from 980 to 1020 nm, from 1170 to 1250 nm, and from 1430 to 1500 nm (Fig. 6), reflecting the thermally induced changes in the physical state of water (Workman & Weyer, 2007). These spectral variations are consistent with previous findings on frozen meat products, such as in the study of frozen beef rounds by Grassi et al. (2024) and they are indicative of the progressive transition of water from liquid to solid state.

Despite compositional differences among the meat cuts, the water-related bands demonstrated similar dynamic behaviour, reinforcing the robustness of these spectral markers for tracking the freezing state in different animal matrices.

To study spectral evolution during the freezing process, PCA was applied separately to the datasets for pork loin, chicken breast and beef

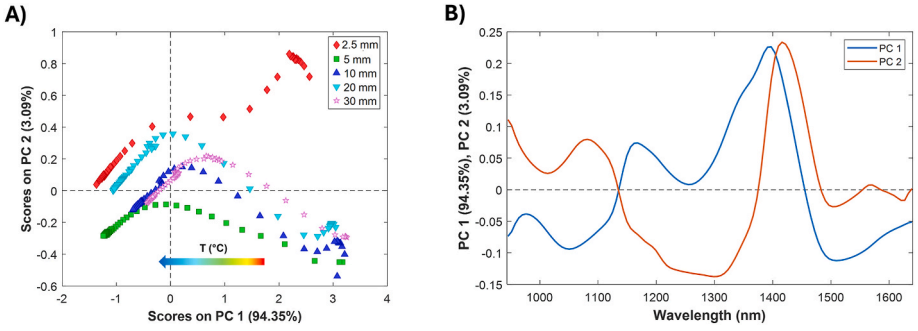

Fig. 4. Score plot (A) and loading plot (B) obtained during the MicroNIR signal penetration depth study on pork loin during the entire process (from refrigerated to frozen), pretreated with smoothing (3 pt) and SNV.

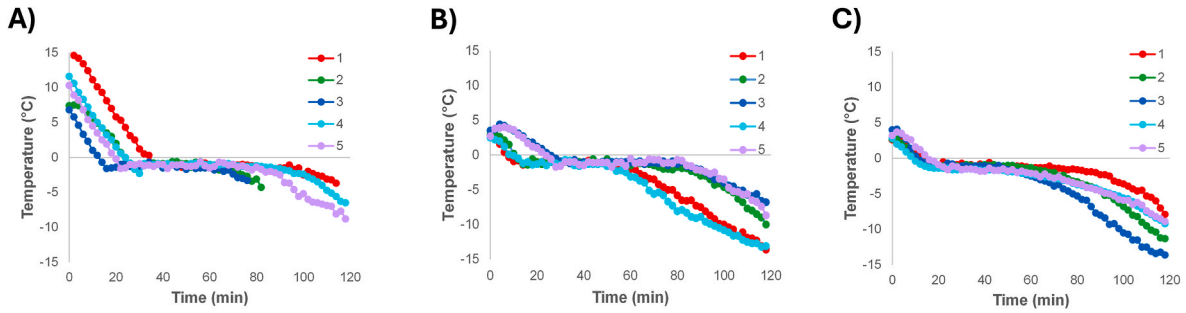

Fig. 5. Temperature profiles recorded at the core of meat cube (A = Pork loin; B = Chicken breast; C = Beef rump) during the superchilling process monitoring across all five trials (from 1 to 5).

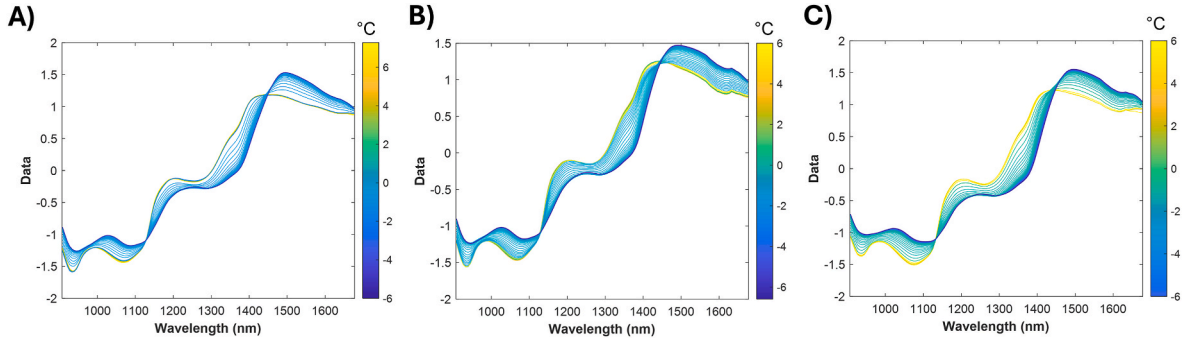

Fig. 6. Spectra collected during the superchilling process monitoring, pretreated with SNV, for one sample each of: A) pork loin, B) Chicken breast, C) Beef rump, coloured according to internal temperature (°C) recorded by temperature probe.

rump, combining each of the five respective tests. Fig. 7A shows the PC1 vs PC2 score plot for the pork loin dataset, selected here as a representative example.

PC1 accounts for most of the total variance (98.09 %) and is mainly associated with progressive spectral changes induced by the transformation of water during freezing. As the internal temperature of the samples decreased, a gradual shift in PC1 scores was observed, reflecting the molecular reorganisation of water during the transition from liquid to solid state. This behaviour is consistent with the expected thermodynamic evolution during freezing and is further confirmed by the PC1 loadings (Fig. 7B), which shows pronounced contributions at ~980 nm, ~1170 nm and ~1400 nm, wavelengths that correspond to known water absorption bands (Workman and Weyer, 2007). This confirmed what previously highlighted by analysing doubly distilled water: the absorption on the low frequency side of the ν_s^{01} (OH) + δ^{01} (OH) (OH stretching and binding) band in a respect to the position of bands maxima is increasing with the temperature decrease (Czarnik-Matusewicz & Pilorz, 2006).

PC2, which describes only 1.2 % of the total variance, showed a clear inverted U-shaped trajectory during the process. At refrigeration temperatures, the samples showed negative PC2 scores. As the internal temperature decreased and the onset of freezing approached, the PC2 scores increased, reaching a maximum. This intermediate phase probably corresponds to the nucleation phase, in which liquid water and ice coexist and the system reaches a temporary energy equilibrium between the two phases. After this phase, as ice crystallisation progressed, PC2 scores decreased dramatically, reflecting a transition to a more homogeneous and stable frozen matrix. This pattern confirms previous results (Grassi et al., 2024) linking PC2 behaviour to the latent heat plateau and the water-ice equilibrium phase. However, it should be notice that the variance described by this component represent a small fraction of the main changes accounted by PC1.

The interpretation is supported by the loadings of PC2 (Fig. 7B), which reveal distinct signals in the same spectral regions associated with water as PC1, but with complementary intensity patterns, reinforcing the hypothesis that PC2 captures dynamic structural changes in water

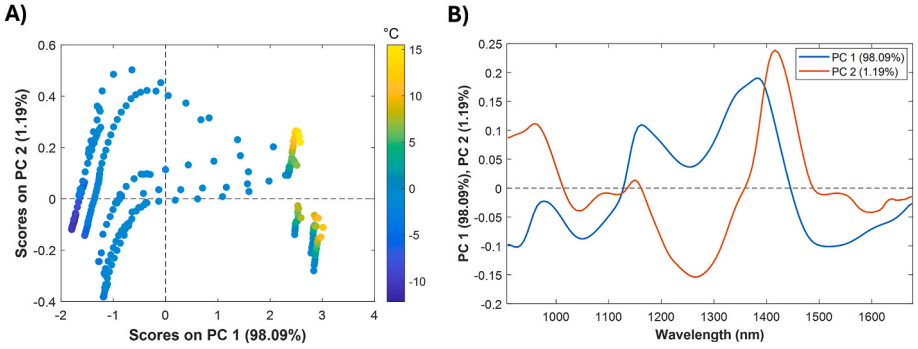

Fig. 7. Score plot (A) and loading plot (B) of pork loin obtained during the superchilling process monitoring (from refrigerated to frozen), pretreated with smoothing (3 pt), SNV and meancentering.

during the critical transition phase.

Although pork loin is used for illustrative purposes, comparable PCA trends and spectral behaviours have been consistently observed in chicken breast and beef rump, confirming the robustness of the dynamics observed in different muscle matrices (Fig. S2).

3.3.3. Aquagram

To better visualise and interpret the structural changes of water during freezing, twelve Water Matrix Coordinates (WAMACs) were selected based on previous literature (Muncan & Tsenkova, 2019). These specific wavelengths correspond to water absorbance bands sensitive to molecular bonding states and they were used to monitor freezing-related spectral variations in pork loin, chicken breast, and beef round (see Table 1 for WAMACs details).

Fig. 8 shows the aquagram profiles for each type of meat (A = pork loin, B = chicken breast, C = beef rump), showing the average variations in absorbance at selected WAMACs during the freezing process. The aquagram illustrates the difference between the spectral signature of water in its liquid state (initial stages of the process) and that of ice-dominated states (later stages), providing a fingerprint of the transformation of water as the temperature decreases.

In all samples, a decrease in absorbance from 1435 nm to 1336 nm (WAMACs from C1 to C7) is observed, associated with the reduction of free OH groups and the formation of hydrogen bonds when water begins to crystallise (Robertson et al., 2003; Xantheas, 1995). This reflects the progressive conversion of water from its less ordered (free) form to a more structured (bound) state. Conversely, WAMACs from C7 to C12 (1435–1509 nm) show an increase in absorbance, indicating improved water bonding and consolidation of the ice structure.

The aquagram encodes each stage of the process with different colours, and the transitions observed are consistent with key thermodynamic events such as ice nucleation and crystal growth (Kaale et al., 2013) and reinforce the temporal resolution of the aquagram in capturing changes in the molecular organisation of water. Thus, the selected WAMACs effectively map the phase transitions of water in the tested muscle tissues.

3.3.4. Development of Multivariate Statistical Control Charts (MSCCs)

In industrial production, it is crucial to monitor the superchilling process to maintain product integrity and ensure quality standards. This study employed NIR spectral data analysis with multivariate statistical process control (MSPC) methods to track freezing events in real-time.

MSPC techniques were applied to identify the start and end points of superchilling events in NIR spectral data. These methods excel in analysing multiple variables simultaneously, detecting subtle variations during superchilling (Bersimis et al., 2007), providing valuable insights into the interaction within the NIR spectral data, enabling precise real-time monitoring of the process. Indeed, for a correct monitoring of the superchilling process should be able to define its main stages: (1) the pre-cooling/chilling stage, i.e. the cooling of the product to its freezing point, and (2) the transition stage, i.e. the removal of the latent heat of crystallisation (Kaale & Eikevik, 2014).

PCA effectively reduces the dimensionality of the data, highlighting key variations during the superchilling process. The PC1 scores were critical in creating a MSCC (Fig. 9), detecting deviations that indicated both the start and the end of the chilling stage.

The start of the chilling stage is characterised by an absolute deviation between PC1 of two consecutive NIR spectra greater than 0.1 as described with formula (1):

$$\left|\frac{\Delta_m}{2}\right| > 0.1 \tag{1}$$

where Δ_{tn} represents the absolute difference between x_{tn} and x_{tn-1}. Considering that x_{tn} is the score of PC1 of the spectrum at instant t_n and x_{tn-1} is the score of PC1 of the spectrum at the previous time t_{n-1}.

The end of the chilling stage, thus the transition stage, was defined as a range of deviation, between −0.01 and 0.01 as described in formula (2):

$$-0.01 < \Delta\Delta_m < 0.01 \tag{2}$$

where $\Delta\Delta_{tn}$ represents the second-order difference in PC1 scores between consecutive NIR spectra.

Aquaphotomics takes advantages of the unique sensitivity of water absorption bands, making it particularly effective in detecting subtle changes in water structure induced by superchilling. Given that the absorption bands related to water vibrations are highly sensitive to physical state changes, C1 scores were utilized to establish a control chart (Fig. 10), like the one previously implemented for PC1. It was determined that the starting point of chilling stage is marked by an absolute deviation between two consecutive NIR spectra exceeding 0.1, consistent with formula (1).

The end point of superchilling was defined by a strait deviation range, between 0 and 0.002, as outlined in formula (3):

$$0 \leq \Delta\Delta_m < 0.002 \tag{3}$$

where $\Delta\Delta_{tn}$ represents the second-order difference in C1 scores between consecutive NIR spectra.

For both control charts, the start of chilling phase is only defined when the condition of formula (1) is satisfied for three consecutive scores, with the start occurring on the first reading. Similarly, for the endpoint, the conditions of formulas (2) and (3) were applied, requiring them to hold for three consecutive scores, with the last occurrence marking the endpoint.

To validate the accuracy of the proposed process monitoring strategy, the start and end points identified by the control charts based on PC1 and C1 scores were compared with reference values derived from thermal data, as summarised in Table 2. To this end, temperature–PC1 plots were analysed to detect thermal transition zones, specifically the temperature values corresponding to the start of nucleation and the completion of the water-ice phase transition. These temperature points were then matched to the corresponding times on the temperature–time profiles. The comparative analysis revealed that the control charts consistently identify both the start and end of the superchilling process with a systematic delay, compared to the method based on thermal observation.

Table 1
Water Matrix Coordinates around the first overtone band in the near-infrared region (1300–1600 nm), adapted from Muncan and Tsenkova (2019).

WAMACS	WL (nm)	Assignment
C1	1336	Asymmetric stretching vibration (V_3) of H_2O
C2	1360	Hydrated OH^- complexes with 1, 2, or 4 water molecules in the solvation shell
C3	1373	Combination band involving symmetric (V_1) and asymmetric (V_3) stretching vibrations of H_2O
C4	1385	OH^- solvated with 1 or 4 water molecules and presence of superoxide $OH^-(H_2O)_4$ species
C5	1398	Free or trapped water molecules, possibly residual solvent
C6	1422	Water hydration involving O–OH bending and O···O intermolecular distances
C7	1435	Water molecules forming a single hydrogen bond (S_1 configuration)
C8	1447	Combination vibration ($V_1 + V_3$) associated with OH^- solvated by 4–5 water molecules
C9	1460	Water molecules forming two hydrogen bonds (S_2 configuration)
C10	1472	Water molecules involved in three hydrogen bonds (S_3 configuration)
C11	1484	Fully coordinated water molecules with four hydrogen bonds (S_4 configuration)
C12	1509	Combination of $V_1 + V_2$ vibrations, associated with strongly bound structural water

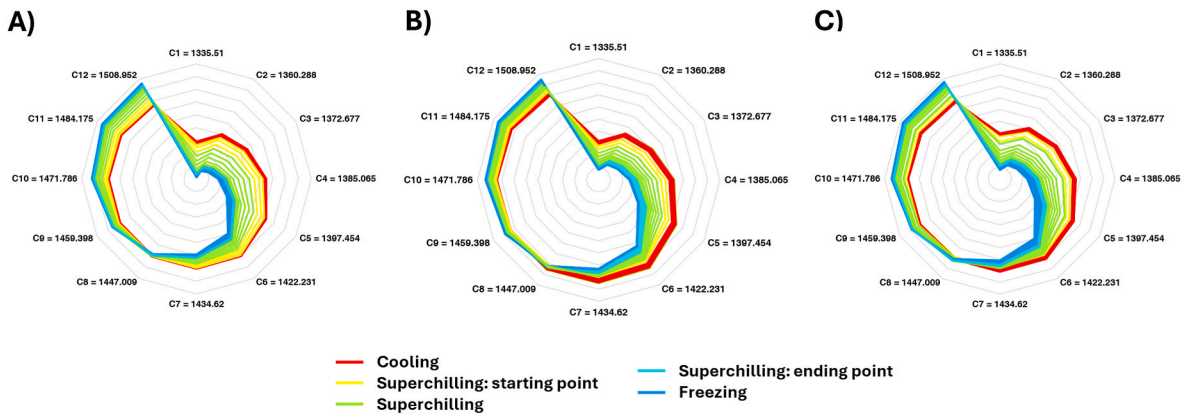

Fig. 8. Aquagram (A = Pork loin; B = Chicken breast; C = Beef rump) with selected WAMACS (nm), coloured according to the process stage during the superchilling process monitoring.

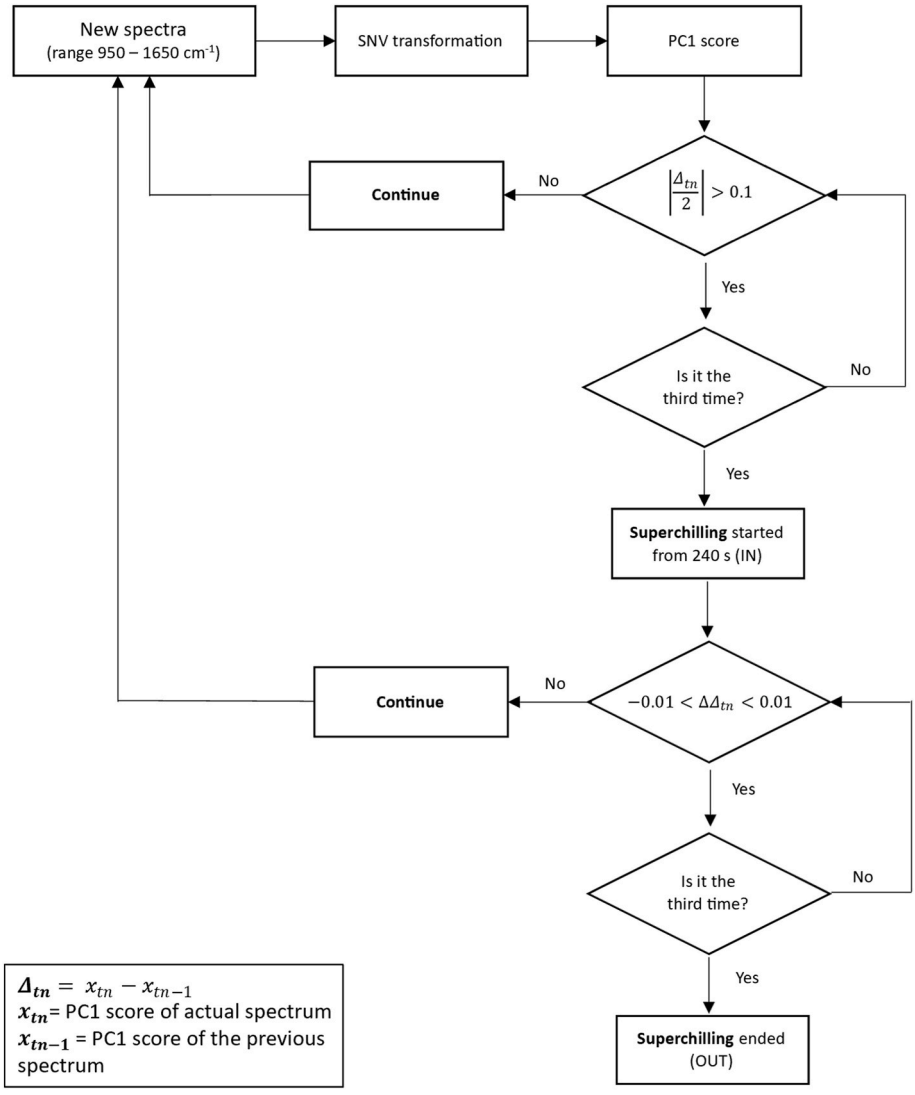

Fig. 9. Control chart on NIR spectra pre-treated with SNV and meancentering, based on PC1 values.

This behaviour is explained by the MSCCs notification criterion, which requires three consecutive measurements to exceed the control limits before setting off an alarm. This introduces a theoretical minimum delay of approximately 6 min. Thus, the real beginning of superchilling transition should be considered 6 min earlier.

Despite this delay, the PC1- and C1-based multivariate control charts demonstrated reliability and robustness, providing an objective, real-time, and automatable system approach to monitor superchilling

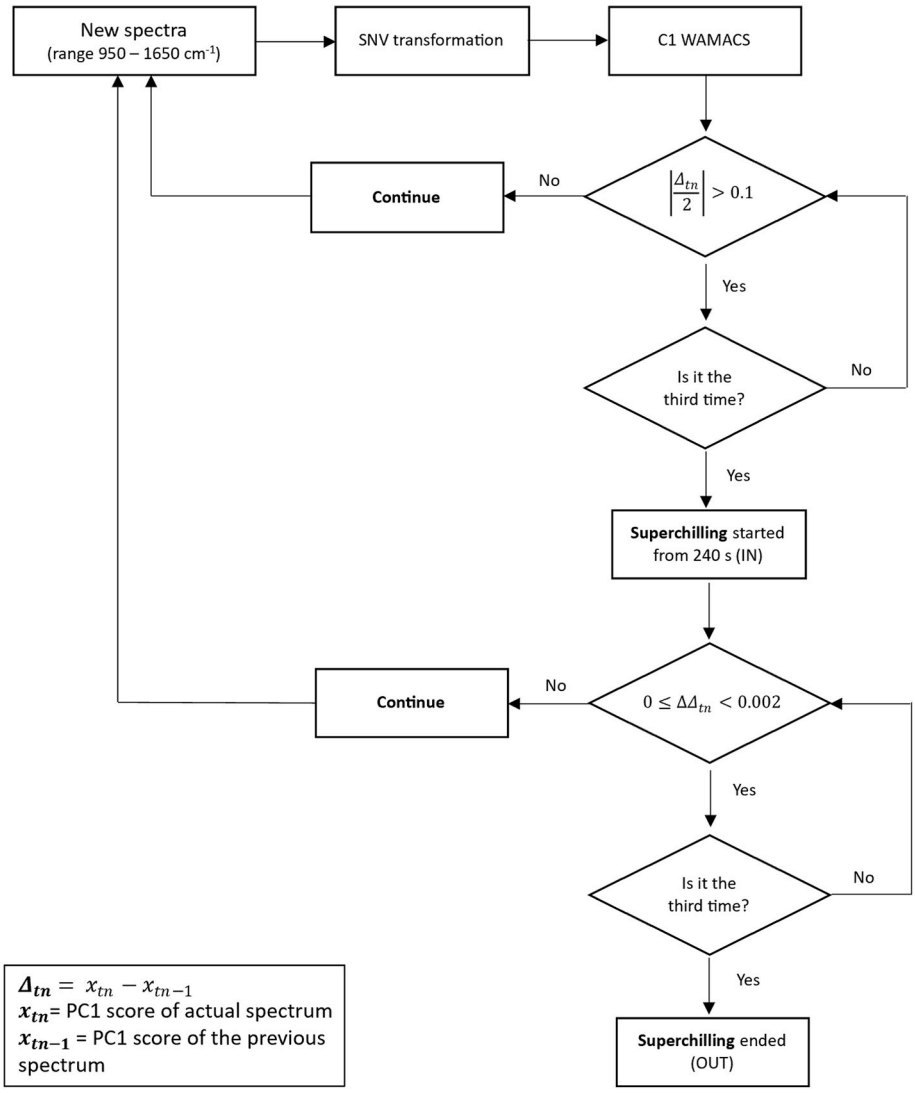

Fig. 10. Control chart on NIR spectra pre-treated with SNV, based on C1 values.

Table 2
Start and end times as determined from the thermal reference method, alongside those calculated using PC1- and C1-based control charts, across all trials and meat cuts.

Meat type	Trial	Temperature		PC1		C1	
		Start (min)	End (min)	Start (min)	End (min)	Start (min)	End (min)
Pork loin	1	36	68	44	64	40	80
	2	28	60	34	60	32	56
	3	16	42	22	50	20	46
	4	30	68	38	54	36	50
	5	22	56	30	62	28	42
Chicken breast	1	56	86	76	104	74	104
	2	16	62	32	56	26	58
	3	34	82	48	82	44	78
	4	14	48	22	48	16	48
	5	28	80	46	78	42	72
Beef rump	1	40	78	56	84	52	80
	2	14	52	22	48	20	46
	3	10	46	12	48	8	40
	4	10	48	14	54	10	50
	5	24	56	32	60	30	58

process.

4. Conclusion

This study explored the potential of NIR spectroscopy, combined with PCA, aquaphotomics and multivariate statistical analysis of data, as a non-destructive tool for monitoring the superchilling process in meat products. Through an experimental project involving pork loin, chicken breast and beef rump, we evaluated both the physical limits of NIR signal penetration and its ability to capture temperature-dependent structural changes in the water within muscle tissue.

Preliminary stability tests have demonstrated that the MicroNIR device remains stable under varying temperature conditions, ensuring the instrument is suitable for process monitoring.

The results confirmed that, under refrigeration conditions, NIR radiation can penetrate the muscle tissue up to 5 mm, while freezing significantly reduces this depth due to increased light scattering. Despite this limitation, the signal proved to be sufficient to penetrate the thin frozen surface layer that typically forms during superchilling, making NIR spectroscopy a viable option for surface analysis in real-time applications.

Furthermore, the spectral evolution recorded during freezing revealed similar trends across all meat cuts. Changes in water-related absorption bands, particularly those around 980, 1200, and 1430 nm,

were closely aligned with the thermodynamic phases of freezing, including ice nucleation and crystal growth. PCA highlighted these transformations, with PC1 reflecting the overall progression of freezing and PC2 capturing the transient equilibrium phase between liquid water and ice.

To further refine the interpretation, aquagrams based on twelve coordinates of the water matrix (WAMAC) provided a clear visualisation of the molecular reorganisation of water during the process. The transition from free water to bound water was evident and consistent across all samples, confirming aquaphotomics as a sensitive and informative approach for detecting physical changes in water structure in biological matrices. Based on this information, multivariate statistical control charts were developed using both PC1 and C1, a specific aquaphotomics marker, enabling real-time identification of the start and end points of superchilling. These models proved to be robust and consistent with thermal references, despite a slight delay introduced by the decision criteria. more frequent spectra sampling would overcome the delay drawback, which can be effectively achieved with the MicroNIR system combined with the MSCC elaboration. Furthermore, this will be useful for faster cooling phase, resulting from more intense cooling conditions. The approach has shown promise for implementation in automated quality control systems, offering objective and timely detection of critical process transitions.

In conclusion, the integration of NIR spectroscopy and multivariate monitoring techniques has proven to be a useful tool for process monitoring in meat. This methodology not only improves the understanding of water dynamics in biological tissues, but also lays the foundation for advanced, non-invasive monitoring tools in the food industry. Future research should aim to optimise these models for complex industrial environments and to explore their application to a wider range of perishable food products, also considering shorter time interval acquisition.

CRediT authorship contribution statement

Irene Locatelli: Writing – original draft, Visualization, Methodology, Investigation, Formal analysis, Data curation. **Silvia Grassi:** Writing – review & editing, Methodology, Investigation, Data curation, Conceptualization.

Funding sources

This research did not receive any specific grant from funding agencies in the public, commercial, or not-for-profit sectors.

Declaration of competing interest

The authors declare that they have no known competing financial interests or personal relationships that could have appeared to influence the work reported in this paper.

Appendix A. Supplementary data

Supplementary data to this article can be found online at https://doi.org/10.1016/j.foodcont.2025.111861.

Data availability

Data will be made available on request.

References

Banerjee, R., & Maheswarappa, N. B. (2019). Superchilling of muscle foods: Potential alternative for chilling and freezing. *Critical Reviews in Food Science and Nutrition, 59*, 1256–1263. https://doi.org/10.1080/10408398.2017.1401975

Bersimis, S., Psarakis, S., & Panaretos, J. (2007). Multivariate statistical process control charts: An overview. *Quality and Reliability Engineering International, 23*, 517–543. https://doi.org/10.1002/qre.829

Collins, J. R. (1925). Change in the infra-red absorption spectrum of water with temperature. *Physical Review, 26*, 771. https://doi.org/10.1103/PhysRev.26.771

Czarnik-Matusewicz, B., & Pilorz, S. (2006). Study of the temperature-dependent near-infrared spectra of water by two-dimensional correlation spectroscopy and principal components analysis. *Vibrational Spectroscopy, 40*, 235–245. https://doi.org/10.1016/j.vibspec.2005.10.002

De Rezende, L. P., Barbosa, J., & Teixeira, P. (2022). Analysis of alternative shelf life-extending protocols and their effect on the preservation of seafood products. *Foods, 11*, 1100. https://doi.org/10.3390/foods11081100

Deepika, S., & Sutar, P. P. (2024). Spectral selective infrared heating of food components based on optical characteristics and penetration depth: A critical review. *Critical Reviews in Food Science and Nutrition, 64*, 10749–10771. https://doi.org/10.1080/10408398.2023.2227899

Ding, D., Zhou, C., Ge, X., Ye, K., Wang, P., Bai, Y., & Zhou, G. (2020). The effect of different degrees of superchilling on shelf life and quality of pork during storage. *Journal of Food Processing and Preservation, 44*, Article e14394. https://doi.org/10.1111/jfpp.14394

Grassi, S., Jiménez, A., Ruiz, J., & González-Mohino, A. (2024). Use of ultrasound and NIRs as tools for monitoring ice formation in superchilled meat. *Journal of Food Engineering, 369*, Article 111957. https://doi.org/10.1016/j.jfoodeng.2024.111957

Huang, Y., Xiong, J., Li, Z., Hu, D., Sun, Y., Jin, H., Zhang, H., & Fang, H. (2024). Recent advances in light penetration depth for postharvest quality evaluation of fruits and vegetables. *Foods, 13*, 2688. https://doi.org/10.3390/foods13172688

Kaale, L. D., & Eikevik, T. M. (2014). The development of ice crystals in food products during the superchilling process and following storage, a review. *Trends in Food Science & Technology, 39*, 91–103. https://doi.org/10.1016/j.tifs.2014.07.004

Kaale, L. D., Eikevik, T. M., Bardal, T., Kjorsvik, E., & Nordtvedt, T. S. (2013). The effect of cooling rates on the ice crystal growth in air-packed salmon fillets during superchilling and superchilled storage. *International Journal of Refrigeration, 36*, 110–119. https://doi.org/10.1016/j.ijrefrig.2012.09.006

Kaale, L. D., Eikevik, T. M., Rustad, T., & Kolsaker, K. (2011). Superchilling of food: A review. *Journal of Food Engineering, 107*, 141–146. https://doi.org/10.1016/j.jfoodeng.2011.06.004

Kim, H., & Hong, G. P. (2022). Comparison of superchilling and supercooling on extending the fresh quality of beef loin. *Foods, 11*, 2729. https://doi.org/10.3390/foods11182729

Kovacs, Z., Muncan, J., Veleva, P., Oshima, M., Shigeoka, S., & Tsenkova, R. (2022). Aquaphotomics for monitoring of groundwater using short-wavelength near-infrared spectroscopy. *Spectrochimica Acta Part A: Molecular and Biomolecular Spectroscopy, 279*, Article 121378. https://doi.org/10.1016/j.saa.2022.121378

Lammertyn, J., Peirs, A., De Baerdemaeker, J., & Nicolaı, B. (2000). Light penetration properties of NIR radiation in fruit with respect to non-destructive quality assessment. *Postharvest Biology and Technology, 18*, 121–132. https://doi.org/10.1016/S0925-5214(99)00071-X

Maeda, H., Ozaki, Y., Tanaka, M., Hayashi, N., & Kojima, T. (1995). Near infrared spectroscopy and chemometrics studies of temperature-dependent spectral variations of water: Relationship between spectral changes and hydrogen bonds. *Journal of Near Infrared Spectroscopy, 3*(4), 191–201. https://opg.optica.org/jnirs/abstract.cfm?URI=jnirs-3-4-191.

Magnussen, O. M., Haugland, A., Hemmingsen, A. K. T., Johansen, S., & Nordtvedt, T. S. (2008). Advances in superchilling of food–process characteristics and product quality. *Trends in Food Science & Technology, 19*, 418–424. https://doi.org/10.1016/j.tifs.2008.04.005

Masoumi, H., Safavi, S. M., & Khani, Z. (2012). Identification and classification of plastic resins using near infrared reflectance. *International Journal of Mechanical and Industrial Engineering, 6*, 213–220. https://doi.org/10.5281/zenodo.1076916

Muncan, J., & Tsenkova, R. (2019). Aquaphotomics—from innovative knowledge to integrative platform in science and technology. *Molecules, 24*, 2742. https://doi.org/10.3390/molecules24152742

Padalkar, M. V., & Pleshko, N. (2015). Wavelength-dependent penetration depth of near infrared radiation into cartilage. *Analyst, 140*, 2093–2100. https://doi.org/10.1039/C4AN01987C

Ramadan, A., Abatzoglou, N., & Gosselin, R. (2025). Addressing temperature variations of miniaturized NIR spectrometers: Advancing quantitative models for pharmaceutical analysis. *Journal of Pharmaceutical and Biomedical Analysis, 264*, Article 116959. https://doi.org/10.1016/j.jpba.2025.116959

Robertson, W. H., Diken, E. G., Price, E. A., Shin, J. W., & Johnson, M. A. (2003). Spectroscopic determination of the OH− solvation shell in the OH−(H2O) n clusters. *Science, 299*, 1367–1372. https://doi.org/10.1126/science.1080695

Roger, J. M., & Boulet, J. C. (2018). A review of orthogonal projections for calibration. *Journal of Chemometrics, 32*, Article e3045. https://doi.org/10.1002/cem.3045

Shiraishi, C. S., Roriz, C. L., Carocho, M., Prieto, M. A., Abreu, R. M., Barros, L., & Heleno, S. A. (2025). Blockchain revolution in food supply chains: A positive impact on global food loss and waste. *Food Chemistry, 467*, Article 142331. https://doi.org/10.1016/j.foodchem.2024.142331

Stevik, A. M., Duun, A. S., Rustad, T., O'Farrell, M., Schulerud, H., & Ottestad, S. (2010). Ice fraction assessment by near-infrared spectroscopy enhancing automated superchilling process lines. *Journal of Food Engineering, 100*, 169–177. https://doi.org/10.1016/j.jfoodeng.2010.03.042

Tsenkova, R., Munćan, J., Pollner, B., & Kovacs, Z. (2018). Essentials of aquaphotomics and its chemometrics approaches. *Frontiers in chemistry, 6*, 363. https://doi.org/10.3389/fchem.2018.00363

Wang, B., Liang, J., Zhou, C., Zhang, J., Ji, L., Li, C., Mei, X., & Chen, H. (2024). Research progress on the effect and mechanism of superchilling preservation technology on meat quality control. *Foods, 13*, 3309. https://doi.org/10.3390/foods13203309

Wold, S., Esbensen, K., & Geladi, P. (1987). Principal component analysis. *Chemometrics and Intelligent Laboratory Systems, 2*, 37–52. https://doi.org/10.1016/0169-7439(87)80084-9

Workman, J. J., & Weyer, L. (2007). *Practical guide to interpretive near-infrared spectroscopy*. CRC press. https://doi.org/10.1201/9781420018318

Xantheas, S. S. (1995). Ab initio studies of cyclic water clusters (H2O) n, n= 1–6. III. Comparison of density functional with MP2 results. *The Journal of Chemical Physics, 102*, 4505–4517. https://doi.org/10.1063/1.469499